

Testing Quantum Mechanics using Noisy Quantum Computers

Kevin Slagle^{1,2}

¹*Department of Physics and Institute for Quantum Information and Matter,
California Institute of Technology,
Pasadena, California 91125, USA*

²*Walter Burke Institute for Theoretical Physics,
California Institute of Technology,
Pasadena, California 91125, USA*

We outline a proposal to test quantum mechanics in the high-complexity regime using noisy intermediate-scale quantum (NISQ) devices. Our procedure involves simulating a non-Clifford random circuit, followed by its inverse, and then checking that the resulting state is the same as the initial state. We are motivated by the hypothesis that quantum mechanics is not fundamental, but instead emerges from a theory with less computational power, such as classical mechanics. This emergent quantum mechanics (EmQM) hypothesis makes the prediction that quantum computers will not be capable of sufficiently complex quantum computations. We show that quantum mechanics predicts that the fidelity of our procedure decays exponentially with circuit depth (due to noise in NISQ devices), while EmQM predicts that the fidelity will decay significantly more rapidly for sufficiently deep circuits, which is the experimental signature that we propose to search for. We estimate rough bounds for when possible signals of EmQM should be expected. We find that useful experiments can be performed with only 80 qubits and gate infidelity 10^{-3} , while highly informative experiments should require only roughly 2000 qubits and gate infidelity 10^{-5} .

Quantum mechanics has enjoyed roughly a century of predictive success. Although there have been many high-precision tests of quantum mechanics [1–3], it is possible that a new experimental regime could discover a breakdown of quantum mechanics: the high-complexity regime of highly entangled states that require deep quantum circuits to prepare. The complexity of a wavefunction can be defined as the number of gates (*e.g.* 2-qubit unitaries) required to make the wavefunction from a product state [4–7]. The high-complexity regime has remained relatively untested since decoherence and noise make it tremendously difficult to probe this regime with high fidelity. We would like to obtain strong evidence for whether or not quantum mechanics breaks down at large complexity scales using a protocol that is appropriate for noisy intermediate-scale quantum (NISQ) [8] devices.

Currently, the leading tests of quantum mechanics in the high-complexity regime were the recent quantum advantage experiments [9–12]. The superconducting qubit experiments [9–11] performed up to 24 layers of random gates on up to 60 qubits, followed by measurements in the computational basis. The infidelity of their circuits can be predicted from, and was verified to be consistent with, the infidelity of the individual gates in the low-complexity regime. This helps verify quantum mechanics up to the regime of 60 qubits entangled by a depth $d = 24$ circuit. However, since the ideal measurement outcomes of their random circuits can not be efficiently calculated on classical computers, it is impractical to extend this methodology to deeper circuits with more qubits. To overcome this, we propose to apply the inverse of the quantum circuit before taking measurements so that the ideal measurement outcome is trivial to calculate.

Our primary motivation is to obtain evidence for or against the hypothesis that quantum mechanics emerges from a local classical theory, which we define as a theory that can be formalized as a (possibly continuous) cellular automaton [13–15]. This possibility is often referred to as emergent quantum mechanics (EmQM) [16], for which there have been several preliminary proposals [14, 17–21]. We are also motivated by recent progress in tensor network [22–27] and neural network [28–31] algorithms and the possibility that future algorithms might yield a model of EmQM. Note that many local classical theories are not local hidden variable theories, which implies that they are not ruled out by Bell experiments; see Appendix E for an explanation.

Since local classical theories can be efficiently simulated on classical computers while classical computers (very likely) can not efficiently simulate quantum mechanics [32–34], models of EmQM must show discrepancies from quantum theory at sufficiently high complexity [17, 35]. However, if quantum mechanics emerges at *e.g.* the Planck scale, then an EmQM theory could effectively have at its disposal one CPU core per Planck volume operating at a Planck frequency. That is an incredible amount of computational power. As such, it is conceivable that a local classical theory could exhibit EmQM well enough to be in agreement with previous experiments, but not the experiment we propose.

I. PROPOSAL

Our proposed protocol, which we summarize in Fig. 1, is to repeat the following:

1. initialize the zero state $|0\rangle$ on n qubits
2. apply d layers of random gates $U_1 \cdots U_d$, with depth d randomly chosen between 0 and d_{\max}
3. apply the inverse $U_d^\dagger \cdots U_1^\dagger$
4. measure in the computational basis and check if the final state is the zero state $|0\rangle$

The max depth d_{\max} should be chosen such that $d_{\max} \gg n^{1/D}$ for a circuit with D -dimensional connectivity (e.g. $d_{\max} \approx 10 n^{1/D}$). Each layer of gates U_t is a product of 2-qubit gates, which are independently and randomly chosen for each sample and layer. The random 2-qubit gates can be chosen from any distribution (of at least two gates¹), as long as the entire forward circuit $U_1 \cdots U_d$ is expected to be difficult to simulate classically. We require that the random distribution for each layer of gates repeats with a small period p ; i.e. U_t and U_{t+p} are independently chosen from the same probability distribution. The depth-dependent fidelity F_d is the fraction of depth- d samples with a measured final state $|0\rangle$. The protocol is complete once the fidelities F_d have been measured to the desired statistical precision.

To make the best use of each sample, each depth d can be sampled with probability $\sim F_d^{-2}$. The circuit depth d is chosen randomly for each sample in order to mitigate the effect of slow drifts in the gate fidelity between samples. (See Appendix C for more on drift.)

We show that quantum mechanics predicts that the fidelity should decay exponentially $F_d \sim e^{-\lambda d}$ with the circuit depth d (until saturation near $F_\infty \sim 2^{-n}$) for Markovian noise models. In contrast, if quantum mechanics emerges from a theory with significantly less computational power, such as classical mechanics, and if λ is sufficiently small to be in the quantum advantage regime [37], then we argue that the fidelity should start to decay significantly faster after a sufficiently large depth d_* , as depicted in Fig. 2.

Our protocol is similar to randomized benchmarking [38–45] and uses a similar mathematical foundation. One difference is that we allow arbitrary non-Clifford gates so that the quantum advantage regime can be reached, while randomized benchmarking typically focuses on Clifford gates so that the inverse unitary can be a low-depth circuit. The low-depth inverse circuit also differs from our proposal since we instead apply a long sequence of

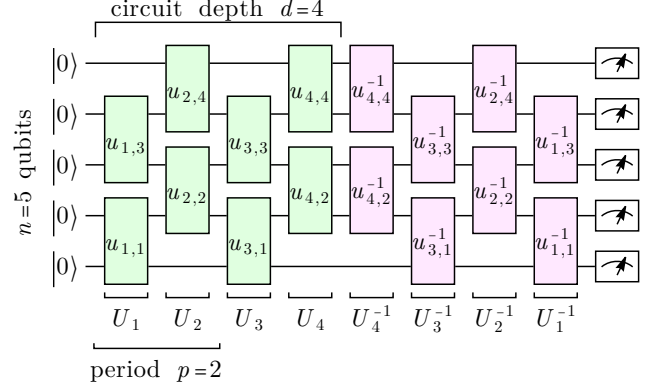


FIG. 1. Our protocol: repeatedly apply a random circuit of a random depth d to n qubits, followed by its inverse, and then measure in the computational basis. For each random sample, the 2-qubit gates $u_{t,i}$ are chosen randomly. The depth-dependent fidelity F_d is the fraction of depth- d samples with final state $|0\rangle$. Although we depict a circuit with one-dimensional connectivity for simplicity, higher-dimensional connectivity is preferable.

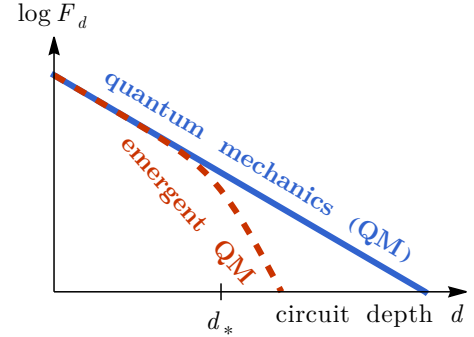


FIG. 2. Exponential fidelity decay $F_d \sim e^{-\lambda d}$ with circuit depth d predicted by quantum mechanics (QM) (blue) vs a schematic sketch of the emergent quantum mechanics (EmQM) expectation (red). EmQM agrees with QM up to a critical depth d_* , after which the EmQM fidelity must start decaying significantly faster (assuming sufficiently large n and small λ).

inverted unitaries in the reverse order (as in a Loschmidt echo [46]), which is typically avoided in randomized benchmarking since it can hide errors [47]. Another difference is that randomized benchmarking typically studies a small number of qubits, while we focus on many $n \gg 1$ qubits. Conveniently, we find that a larger number of qubits helps make the exponential fidelity decay cleaner.

¹ Using random instead of fixed gates reduces fluctuations in the exponential fidelity decay that result from coherent errors [36].

II. EmQM EXPECTATION

We expect that an EmQM theory would not have enough computational power to accurately perform the forward circuit (green in Fig. 1) of our protocol for sufficiently many qubits n and large depth d . In particular, we assume that if the zero state $|0\rangle$ is measured at the end of the protocol, then an EmQM would have had to simulate the circuit well enough such that the EmQM could also randomly sample bit strings from the forward circuit (*i.e.* bit strings b from the probability distribution $P(b) = |\langle b | U_d \cdots U_1 | 0 \rangle|^2$). This is the same sampling task considered in recent quantum advantage experiments [9–11] and is expected to require an exponential amount of CPU time for classical algorithms [48–52]. Building on these assumptions, we can roughly predict when our protocol might see signals of EmQM.

Consider the brute-force Schrödinger algorithm (SA) [53], which involves simply applying unitary matrices to a 2^n -component wavefunction. This algorithm can simulate a depth d circuit of n qubits in $N_{\text{CPU}}^{\text{SA}} \approx nd 2^n \sim 2^n$ CPU cycles. We are not aware of any faster algorithms that could sample bit strings from random D -dimensional non-Clifford circuits with large depth $d \gg n^{1/D} \gg 1$ and large gate fidelity² (even if only a small circuit fidelity $F \sim 10^{-3}$ is required) [10, 33, 48, 52].

Suppose that a quantum computer performs such a circuit within length and times scales L_{QPU} and T_{QPU} . Further assume that quantum mechanics emerges at length and time scales L_{EmQM} and T_{EmQM} . Being a local classical theory, an EmQM theory can be simulated in real time using roughly one CPU core per $L_{\text{EmQM}}^{D_{\text{EmQM}}}$ volume operating at frequency T_{EmQM}^{-1} . D_{EmQM} is the number of spatial dimensions, which could be greater than three if there are extra spatial dimensions. Therefore, an algorithm simulating the EmQM theory could simulate the circuit with $N_{\text{CPU}}^{\text{EmQM}} \sim \frac{T_{\text{QPU}}}{T_{\text{EmQM}}} \left(\frac{L_{\text{QPU}}}{L_{\text{EmQM}}} \right)^{D_{\text{EmQM}}} \text{CPU cycles}$.

By applying our expectation that no algorithm is faster than the Schrödinger algorithm, we can bound $N_{\text{CPU}}^{\text{SA}} \lesssim N_{\text{CPU}}^{\text{EmQM}}$ and then solve for n in $2^n \sim N_{\text{CPU}}^{\text{SA}} \lesssim N_{\text{CPU}}^{\text{EmQM}}$ to estimate the largest number of qubits n_* that an EmQM theory could accurately handle at large depth:

$$\begin{aligned} n_* &\lesssim \log_2 \frac{T_{\text{QPU}}}{T_{\text{EmQM}}} + D_{\text{EmQM}} \log_2 \frac{L_{\text{QPU}}}{L_{\text{EmQM}}} \\ &\lesssim 130 + \log_2 \frac{T_{\text{P}}}{T_{\text{EmQM}}} + D_{\text{EmQM}} \left(110 + \log_2 \frac{L_{\text{P}}}{L_{\text{EmQM}}} \right) \end{aligned} \quad (1)$$

Therefore when $n \geq n_*$, there should be a critical depth d_* after which any EmQM theory should deviate from

quantum mechanics predictions (as in Fig. 2). As an example, we express the second line relative to Planck length L_{P} and time T_{P} scales with $L_{\text{QPU}} \sim 1$ centimeter and $T_{\text{QPU}} \sim 10^{-3}$ seconds. Note that Eq. (1) is remarkably predictive because huge changes in these unknown scales only modestly affect our bound on n_* due to the logarithmic dependence. In particular, only $n_* \lesssim 2000$ qubits may be needed to significantly rule out the EmQM hypothesis (if we assume $D_{\text{EmQM}} \leq 6$, $T_{\text{EmQM}} \geq 10^{-50} T_{\text{P}}$, and $L_{\text{EmQM}} \geq 10^{-50} L_{\text{P}}$).³

In order to bound n_* using the Schrödinger algorithm argument, we had to assume $d \gg n^{1/D} \gg 1$. Therefore we can roughly bound the critical depth $d_* \lesssim n_*^{1/D}$. In an attempt to safely exceed this bound, we consider max circuit depths $d_{\text{max}} \approx 10 n^{1/D}$ for which it seems likely that $d_{\text{max}} > d_*$.

With $N_{\text{s}} = 10^8$ samples, the fidelity can be measured down to $F_{\text{min}} \approx N_{\text{s}}^{-1/2} \epsilon_{\text{r}}^{-1} \approx 10^{-3}$ with a relative error of $\epsilon_{\text{r}} \approx 10\%$. We will show that if each 2-qubit gate has an entanglement fidelity^[56] f , then quantum mechanics predicts that our protocol has fidelity $F_d \sim f^{nd}$, where nd is the approximate number of 2-qubit gates. Therefore, statistically significant data can be obtained for $nd \lesssim \frac{\ln F_{\text{min}}}{\ln f} \approx \frac{\ln F_{\text{min}}^{-1}}{1-f}$.

For $D = 2$ dimensional circuits with gate infidelity $1 - f = 10^{-3}$ and $F_{\text{min}} = 10^{-3}$, statistical significance requires $nd \lesssim 7000$, *i.e.* a maximum of $n \approx 80$ if $d_{\text{max}} \approx 10 n^{1/D} \approx 90$ (which is significantly larger than the $n \approx 60$ and $d \approx 24$ used in Refs. [9–11]). With gate infidelity $1 - f = 0.8 \times 10^{-5}$ (which may require error correction techniques [57]) and $F_{\text{min}} = 10^{-3}$, statistical significance requires $nd \lesssim 8.6 \times 10^5$, *i.e.* a maximum of $n \approx 2000$ if $d_{\text{max}} \approx 10 n^{1/D} \approx 440$, which could rule out the EmQM hypothesis with higher confidence.

III. QUANTUM MECHANICS PREDICTION

We now argue that quantum mechanics predicts that the fidelity F_d decays exponentially with circuit depth d under physically reasonable noise models. Intuitively, each gate u has a probability p_u of making an error, resulting in a gate entanglement fidelity $f_u \approx 1 - p_u$. Intuitively, the fidelity F_d is then roughly the probability f^{nd} that none of the $\approx nd$ two-qubit gates made an error:

$$F_d \sim \tilde{F}_0 e^{-\lambda d} \quad (2)$$

where $\lambda \sim -n \ln f$ and f is an average gate entanglement fidelity (until the fidelity eventually saturates near

² Gate fidelity above the error-correction threshold $f \approx 0.99$ [54, 55] is presumably sufficient

³ L_{QPU} and T_{QPU} do not significantly affect this estimate. For example, increasing these values to $T_{\text{QPU}} = 100$ years and $L_{\text{QPU}} = 100$ light-years only increases our estimated bound on n_* by $42 + 66 D_{\text{EmQM}}$.

$F_\infty \sim 2^{-n}$). In the experiment, \tilde{F}_0 and λ are fitting parameters. We substantiate this intuition below. In Appendix A, we provide additional evidence that the fidelity should decay exponentially (according to quantum mechanics) using a 2-design twirling argument.

As a first approximation, we model the fidelity using gate-dependent but time-independent noise:

$$F_d = \mathbb{E}_{U_1, \dots, U_d} \text{tr}[\rho^{\text{fin}} (\Phi_{U_1^\dagger} \circ \dots \circ \Phi_{U_d^\dagger} \circ \Phi_{U_d} \circ \dots \circ \Phi_{U_1})(\rho^{\text{init}})] \quad (3)$$

The initial state is modeled by a density matrix ρ^{init} . Measuring if the final state is the zero state is modeled by the quantum channel $\rho \rightarrow \text{tr}(\rho^{\text{fin}} \rho)$. ρ^{init} and ρ^{fin} are close to the n -qubit zero state $|0\rangle\langle 0|$, up to some infidelity resulting from state preparation and measurement (SPAM) errors. $\mathbb{E}_{U_1, \dots, U_d}$ averages over the allowed layers of random gates. The quantum channel Φ_{U_t} models the noisy quantum computer implementation for a particular layer of random gates U_t .

As depicted in Fig. 1, each layer of gates U_t is a product of 2-qubit gates $U_t = \prod_i u_{t,i}$, where i labels a pair of qubits. We similarly model the quantum channel Φ_{U_t} as a composition of noisy quantum channels: $\Phi_{U_t} = \circ_i \Phi_{u_{t,i}}$. Each 2-qubit channel Φ_u can be decomposed as $\Phi_u(\rho) = \mathcal{N}_u(u\rho u^\dagger)$, where the noise channel \mathcal{N}_u depends on the unitary u and the two qubits that it acts on.

We expand the noise channel for each gate as⁴:

$$\mathcal{N}_u(\rho) = \sum_{\alpha, \beta \in \{0,1,2,3\}^2} \chi_{\alpha\beta}^{(u)} \sigma_\alpha \rho \sigma_\beta \quad (4)$$

where $\chi^{(u)}$ is a positive semi-definite matrix and $\sigma_\alpha \in \{I, X, Y, Z\}^{\otimes 2}$ is a 2-qubit Pauli operator. The gate entanglement fidelity^[56] $f_u = \chi_{00}^{(u)}$ plays an important role since all other terms in the expansion result in an error and very small fidelity. For large gate fidelities ($f_u \approx 1$), errors (for which $\alpha \neq 0$ or $\beta \neq 0$) are suppressed by small $|\chi_{\alpha\beta \neq 00}^{(u)}| \leq \sqrt{1 - f_u}$.^[60] Therefore multiple errors will typically be separated by many gates, which will spread out [61–64] any non-identity σ_α or σ_β factor into a highly non-local operator. After spreading out, the contribution to the fidelity in Eq. (3) resulting from one or more errors is very small $O(2^{-n})$.^[65] For a large number of qubits n , any error will typically result in a negligible contribution to the fidelity.

Therefore, the fidelity F_d in Eq. (3) is roughly the fraction of times that no error occurs. $F_0 = \text{tr} \rho^{\text{fin}} \rho^{\text{init}}$ is the probability that a SPAM error occurred. The probability that no error occurs during the forward and

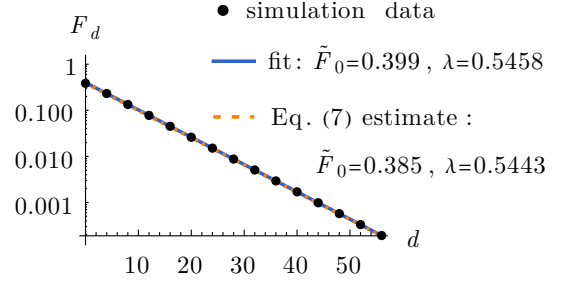


FIG. 3. Simulation data (black dots) showing the quantum mechanics prediction of the exponential fidelity F_d decay for a 5×5 grid of $n = 25$ noisy qubits. Also shown is a fit (blue line) to an exponential decay [Eq. (2)] and the rough predictions (dotted orange line) from Eq. (7).

backward 2-qubit gates $u_{t,i}$ and $u_{t,i}^\dagger$ is

$$f_i^2 = \mathbb{E}_{u_{t,i}} f_{u_{t,i}} f_{u_{t,i}^\dagger} \quad (5)$$

where $\mathbb{E}_{u_{t,i}}$ averages over the allowed 2-qubit gates. Therefore, the probability that no errors occur over the entire circuit of $2n_g d/p$ gates is roughly

$$F_d \sim F_0 f^{2n_g d/p} \quad \text{with} \quad f^{2n_g} = \prod_{i=1}^{n_g} f_i^2 \quad (6)$$

where f is an average gate entanglement fidelity and n_g is the number of gates in a period (e.g. $n_g = 4$ in Fig. 1). We thus obtain Eq. (2) with

$$\tilde{F}_0 \approx F_0 = \text{tr} \rho^{\text{fin}} \rho^{\text{init}} \quad \lambda \approx -\frac{2n_g}{p} \ln f \quad (7)$$

where λ reduces to $\lambda \sim -n \ln f$ when $n_g \sim pn/2$, as is typically the case.

Although Eq. (7) is only an approximate expression for \tilde{F}_0 and λ since multiple errors can sometimes cancel out (especially if they are spatially close or at mirrored positions in the circuit), we numerically find that Eq. (7) is a very good approximation for many qubits $n \gg 1$ and large gate fidelity $f \approx 1$. As an example, in Fig. 3 we show a simulation for a 5×5 grid of $n = 25$ qubits using roughly Sycamore/Zuchongzhi-like [9, 10] gates with gate-dependent errors and average gate entanglement fidelity $f \approx 0.993$ using the Markovian model Eq. (3). (See Appendix B for details.)

IV. EXAMPLE: EmQM FROM MPS

It is illuminating to consider the time evolution of matrix product states (MPS) [66] with fixed bond dimension as an (incomplete) toy model of emergent quantum mechanics (EmQM) in one spatial dimension. We do not consider MPS to be a legitimate model

⁴ n -qubit noise channels could alternatively be considered to model cross-talk [58] or cosmic ray [59] errors with minimal changes to our arguments.

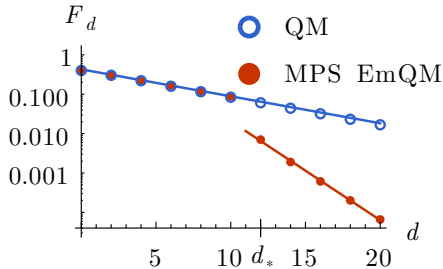


FIG. 4. Simulation data (red dots) showing the fidelity F_d decay of a matrix product state (MPS) toy model of EmQM with bond dimension $\chi = 2^{10}$ for a chain of 24 noisy qubits. Similar to Fig. 2, the toy EmQM theory agrees with the quantum mechanics (QM) prediction (blue circles) until a critical depth $d_* = 12$, after which the fidelity decays at a significantly faster exponential rate. Lines are fits to these two regimes.

of EmQM because it is currently not known how to generalize MPS algorithms to a three-dimensional local classical theory that could be compatible with previous experiments (see Appendix D); although there has been remarkable related algorithmic progress [23–25, 67].

In Fig. 4, we show a MPS simulation of our protocol with noisy gates (similar to Fig. 3) for a chain of 24 qubits. (See Appendix B 4 for details.) During the MPS simulation, bond dimensions are truncated to $\chi \leq 2^{10}$, which limits the amount of Rényi-0 entanglement entropy [68] across any cut of the chain. The maximum entanglement is reached at the critical depth d_* , after which the fidelity decay is dominated by the truncation error [37] of the MPS algorithm (instead of the gate infidelity) and the fidelity F_d begins to decay at a faster exponential rate. This is precisely the EmQM signature depicted in Fig. 2.

V. DISCUSSION

If an exponential fidelity decay (blue in Fig. 2) is observed for high-depth circuits on many qubits, then our arguments in Sec. II will significantly rule out possible theories of emergent quantum mechanics (EmQM), including Refs. [14, 17–21]. Since our proposed experiment requires making several assumptions, once more fault tolerant quantum computers are available, it will be useful to further verify quantum mechanics using verification protocols [69–71] or Shor’s algorithm [72, 73].

If a signal suggestive of EmQM (red in Fig. 2) is experimentally observed, then future work will be required to either determine what the true underlying theory is or rule out explanations consistent with quantum mechanics (*e.g.* non-Markovian noise or state leakage [74, 75]).

If quantum mechanics does emerge from a local

classical theory, then the computational power of quantum computers could be severely limited [17, 35]. For example, **BQP** problems would only be tractable for limited problem sizes. Nevertheless, quantum computers would still be incredibly useful technology, particularly as a device to probe new fundamental physics.

However, it is possible that violations of quantum mechanics could make quantum computers more powerful for certain tasks. For example, if it is possible to violate the probabilistic Born’s rule such that postselection could be performed, then quantum computers may be able to efficiently solve problems in the **PostBQP** = **PP** [32, 76] complexity class up to a bounded problem size. This could be possible if the EmQM prefers to drop branches of the wavefunction with a complexity that is too high⁵ (which would be a possible mechanism behind the EmQM signature of rapid fidelity decay).

We thank John Preskill, Alex Dalzell, Andru Gheorghiu, Ulysse Chabaud, Sean Carroll, Spiros Michalakis, Vitaly Vanchurin, Leonid Pryadko, Xie Chen, and Natalie Klco for helpful conversations. K.S. is supported by the Walter Burke Institute for Theoretical Physics at Caltech; and the U.S. Department of Energy, Office of Science, National Quantum Information Science Research Centers, Quantum Science Center.

-
- [1] S. K. Lamoreaux, A review of the experimental tests of quantum mechanics, *International Journal of Modern Physics A* **07**, 6691 (1992).
 - [2] E. S. Fry and T. Walther, Fundamental tests of quantum mechanics, *Advances In Atomic, Molecular, and Optical Physics*, **42**, 1 (2000).
 - [3] P. Shadbolt, J. C. F. Mathews, A. Laing, and J. L. O’Brien, Testing foundations of quantum mechanics with photons, *Nature Physics* **10**, 278 (2014), [arXiv:1501.03713](#).
 - [4] A. R. Brown and L. Susskind, Second law of quantum complexity, *Phys. Rev. D* **97**, 086015 (2018), [arXiv:1701.01107](#).
 - [5] L. Susskind, Black Holes and Complexity Classes, (2018), [arXiv:1802.02175](#).
 - [6] F. G. S. L. Brandão, W. Chemissany, N. Hunter-Jones, R. Kueng, and J. Preskill, Models of quantum complexity growth, (2019), [arXiv:1912.04297](#).
 - [7] J. Haferkamp, P. Faist, N. B. T. Kothakonda, J. Eisert, and N. Yunger Halpern, Linear growth of quantum circuit complexity, (2021), [arXiv:2106.05305](#).

⁵ To exploit this, consider a quantum computer in a superposition of orthogonal states $|\psi_1\rangle + |\psi_2\rangle$ consisting of many qubits ($n > n_*$) but complexity below the critical complexity. Then maybe one could postselect the $|\psi_1\rangle$ state by applying a controlled high-depth random unitary U to only the $|\psi_2\rangle$ component:

$$|\psi_1\rangle + |\psi_2\rangle \xrightarrow{\text{controlled-}U} |\psi_1\rangle + U|\psi_2\rangle \xrightarrow{\text{EmQM drops } U|\psi_2\rangle} |\psi_1\rangle.$$

- [8] J. Preskill, Quantum Computing in the NISQ era and beyond, *Quantum* **2**, 79 (2018), [arXiv:1801.00862](#).
- [9] F. Arute, K. Arya, R. Babbush, D. Bacon, J. C. Bardin, R. Barends, R. Biswas, S. Boixo, F. G. S. L. Brandao, D. A. Buell, B. Burkett, Y. Chen, Z. Chen, B. Chiaro, R. Collins, W. Courtney, A. Dunsworth, E. Farhi, B. Foxen, A. Fowler, C. Gidney, M. Giustina, R. Graff, K. Guerin, S. Habegger, M. P. Harrigan, M. J. Hartmann, A. Ho, M. Hoffmann, T. Huang, T. S. Humble, S. V. Isakov, E. Jeffrey, Z. Jiang, D. Kafri, K. Kechedzhi, J. Kelly, P. V. Klimov, S. Knysh, A. Korotkov, F. Kostitsa, D. Landhuis, M. Lindmark, E. Lucero, D. Lyakh, S. Mandrà, J. R. McClean, M. McEwen, A. Megrant, X. Mi, K. Michielsen, M. Mohseni, J. Mutus, O. Naaman, M. Neeley, C. Neill, M. Y. Niu, E. Ostby, A. Petukhov, J. C. Platt, C. Quintana, E. G. Rieffel, P. Roushan, N. C. Rubin, D. Sank, K. J. Satzinger, V. Smelyanskiy, K. J. Sung, M. D. Trevithick, A. Vainsencher, B. Villalonga, T. White, Z. J. Yao, P. Yeh, A. Zalcman, H. Neven, and J. M. Martinis, Quantum supremacy using a programmable superconducting processor, *Nature* **574**, 505–510 (2019).
- [10] Y. Wu, W.-S. Bao, S. Cao, F. Chen, M.-C. Chen, X. Chen, T.-H. Chung, H. Deng, Y. Du, D. Fan, M. Gong, C. Guo, C. Guo, S. Guo, L. Han, L. Hong, H.-L. Huang, Y.-H. Huo, L. Li, N. Li, S. Li, Y. Li, F. Liang, C. Lin, J. Lin, H. Qian, D. Qiao, H. Rong, H. Su, L. Sun, L. Wang, S. Wang, D. Wu, Y. Xu, K. Yan, W. Yang, Y. Yang, Y. Ye, J. Yin, C. Ying, J. Yu, C. Zha, C. Zhang, H. Zhang, K. Zhang, Y. Zhang, H. Zhao, Y. Zhao, L. Zhou, Q. Zhu, C.-Y. Lu, C.-Z. Peng, X. Zhu, and J.-W. Pan, Strong quantum computational advantage using a superconducting quantum processor, (2021), [arXiv:2106.14734](#).
- [11] Q. Zhu, S. Cao, F. Chen, M.-C. Chen, X. Chen, T.-H. Chung, H. Deng, Y. Du, D. Fan, M. Gong, C. Guo, C. Guo, S. Guo, L. Han, L. Hong, H.-L. Huang, Y.-H. Huo, L. Li, N. Li, S. Li, Y. Li, F. Liang, C. Lin, J. Lin, H. Qian, D. Qiao, H. Rong, H. Su, L. Sun, L. Wang, S. Wang, D. Wu, Y. Wu, Y. Xu, K. Yan, W. Yang, Y. Yang, Y. Ye, J. Yin, C. Ying, J. Yu, C. Zha, C. Zhang, H. Zhang, K. Zhang, Y. Zhang, H. Zhao, Y. Zhao, L. Zhou, C.-Y. Lu, C.-Z. Peng, X. Zhu, and J.-W. Pan, Quantum Computational Advantage via 60-Qubit 24-Cycle Random Circuit Sampling, (2021), [arXiv:2109.03494](#).
- [12] H.-S. Zhong, H. Wang, Y.-H. Deng, M.-C. Chen, L.-C. Peng, Y.-H. Luo, J. Qin, D. Wu, X. Ding, Y. Hu, P. Hu, X.-Y. Yang, W.-J. Zhang, H. Li, Y. Li, X. Jiang, L. Gan, G. Yang, L. You, Z. Wang, L. Li, N.-L. Liu, C.-Y. Lu, and J.-W. Pan, Quantum computational advantage using photons, *Science* **370**, 1460 (2020), [arXiv:2012.01625](#).
- [13] S. Wolfram, *A New Kind of Science* (2002).
- [14] G. 't Hooft, Deterministic Quantum Mechanics: the Mathematical Equations, (2020), [arXiv:2005.06374](#).
- [15] G. 't Hooft, Ontology in quantum mechanics, (2021), [arXiv:2107.14191](#).
- [16] J. Walleczek and G. Grössing, Is the World Local or Nonlocal? Towards an Emergent Quantum Mechanics in the 21st Century, in *Journal of Physics Conference Series*, Journal of Physics Conference Series, Vol. 701 (2016) p. 012001, [arXiv:1603.02862](#).
- [17] G. 't Hooft, The Cellular Automaton Interpretation of Quantum Mechanics, (2014), [arXiv:1405.1548](#).
- [18] S. L. Adler, Quantum theory as an emergent phenomenon: Foundations and phenomenology, *Journal of Physics: Conference Series* **361**, 012002 (2012).
- [19] V. Vanchurin, Entropic Mechanics: Towards a Stochastic Description of Quantum Mechanics, *Foundations of Physics* **50**, 40 (2019), [arXiv:1901.07369](#).
- [20] V. Vanchurin, The world as a neural network, *Entropy* **22**, 10.3390/e22111210 (2020), [arXiv:2008.01540](#).
- [21] M. I. Katsnelson and V. Vanchurin, Emergent Quantumness in Neural Networks, (2020), [arXiv:2012.05082](#).
- [22] R. Orús, Tensor networks for complex quantum systems, *Nature Reviews Physics* **1**, 538 (2019), [arXiv:1812.04011](#).
- [23] M. P. Zaletel and F. Pollmann, Isometric Tensor Network States in Two Dimensions, *Phys. Rev. Lett.* **124**, 037201 (2020), [arXiv:1902.05100](#).
- [24] K. Hyatt and E. M. Stoudenmire, DMRG Approach to Optimizing Two-Dimensional Tensor Networks, (2019), [arXiv:1908.08833](#).
- [25] R. Haghshenas, M. J. O'Rourke, and G. K.-L. Chan, Conversion of projected entangled pair states into a canonical form, *Phys. Rev. B* **100**, 054404 (2019), [arXiv:1903.03843](#).
- [26] A. J. Ferris, Unbiased Monte Carlo for the age of tensor networks, (2015), [arXiv:1507.00767](#).
- [27] K. Slagle, In preparation.
- [28] I. López Gutiérrez and C. B. Mendl, Real time evolution with neural-network quantum states, (2019), [arXiv:1912.08831](#).
- [29] M. Schmitt and M. Heyl, Quantum Many-Body Dynamics in Two Dimensions with Artificial Neural Networks, *Phys. Rev. Lett.* **125**, 100503 (2020), [arXiv:1912.08828](#).
- [30] S.-H. Lin and F. Pollmann, Scaling of neural-network quantum states for time evolution, (2021), [arXiv:2104.10696](#).
- [31] B. Jónsson, B. Bauer, and G. Carleo, Neural-network states for the classical simulation of quantum computing, (2018), [arXiv:1808.05232](#).
- [32] M. J. Bremner, R. Jozsa, and D. J. Shepherd, Classical simulation of commuting quantum computations implies collapse of the polynomial hierarchy, *Proceedings of the Royal Society of London Series A* **467**, 459 (2011), [arXiv:1005.1407](#).
- [33] S. Aaronson and L. Chen, Complexity-Theoretic Foundations of Quantum Supremacy Experiments, (2016), [arXiv:1612.05903](#).
- [34] S. Boixo, S. V. Isakov, V. N. Smelyanskiy, R. Babbush, N. Ding, Z. Jiang, M. J. Bremner, J. M. Martinis, and H. Neven, Characterizing quantum supremacy in near-term devices, *Nature Physics* **14**, 595–600 (2018), [arXiv:1608.00263](#).
- [35] G. 't Hooft, Quantum gravity as a dissipative deterministic system, *Classical and Quantum Gravity* **16**, 3263 (1999), [arXiv:gr-qc/9903084](#).
- [36] J. J. Wallman and J. Emerson, Noise tailoring for scalable quantum computation via randomized compiling, *Phys. Rev. A* **94**, 052325 (2016), [arXiv:1512.01098](#).
- [37] Y. Zhou, E. M. Stoudenmire, and X. Waintal, What Limits the Simulation of Quantum Computers?, *Physical Review X* **10**, 041038 (2020), [arXiv:2002.07730](#).
- [38] J. Emerson, R. Alicki, and K. Życzkowski, Scalable noise estimation with random unitary operators, *Journal of Optics B: Quantum and Semiclassical Optics* **7**, S347

- (2005), [arXiv:quant-ph/0503243](#).
- [39] C. Dankert, R. Cleve, J. Emerson, and E. Livine, Exact and approximate unitary 2-designs and their application to fidelity estimation, *Phys. Rev. A* **80**, 012304 (2009), [arXiv:quant-ph/0606161](#).
- [40] E. Magesan, J. M. Gambetta, and J. Emerson, Scalable and Robust Randomized Benchmarking of Quantum Processes, *Phys. Rev. Lett.* **106**, 180504 (2011), [arXiv:1009.3639](#).
- [41] E. Magesan, J. M. Gambetta, and J. Emerson, Characterizing quantum gates via randomized benchmarking, *Phys. Rev. A* **85**, 042311 (2012), [arXiv:1109.6887](#).
- [42] J. J. Wallman, Randomized benchmarking with gate-dependent noise, *Quantum* **2**, 47 (2018), [arXiv:1703.09835](#).
- [43] E. Knill, D. Leibfried, R. Reichle, J. Britton, R. B. Blakestad, J. D. Jost, C. Langer, R. Ozeri, S. Seidelin, and D. J. Wineland, Randomized benchmarking of quantum gates, *Phys. Rev. A* **77**, 012307 (2008), [arXiv:0707.0963](#).
- [44] J. Helsen, I. Roth, E. Onorati, A. H. Werner, and J. Eisert, A general framework for randomized benchmarking, (2020), [arXiv:2010.07974](#).
- [45] Y. Liu, M. Otten, R. Bassirianjahromi, L. Jiang, and B. Fefferman, Benchmarking near-term quantum computers via random circuit sampling, (2021), [arXiv:2105.05232](#).
- [46] T. Gorin, T. Prosen, T. H. Seligman, and M. Žnidarič, Dynamics of Loschmidt echoes and fidelity decay, *Phys. Rep.* **435**, 33 (2006), [arXiv:quant-ph/0607050](#).
- [47] R. Shaffer, E. Megidish, J. Broz, W.-T. Chen, and H. Häffner, Practical verification protocols for analog quantum simulators, *npj Quantum Information* **7**, 46 (2021), [arXiv:2003.04500](#).
- [48] A. W. Harrow and A. Montanaro, Quantum computational supremacy, *Nature (London)* **549**, 203 (2017), [arXiv:1809.07442](#).
- [49] R. Movassagh, Quantum supremacy and random circuits, (2019), [arXiv:1909.06210](#).
- [50] A. Bouland, B. Fefferman, C. Nirkhe, and U. Vazirani, On the complexity and verification of quantum random circuit sampling, *Nature Physics* **15**, 159–163 (2019), [arXiv:1803.04402](#).
- [51] S. Aaronson and S. Gunn, On the Classical Hardness of Spoofing Linear Cross-Entropy Benchmarking, (2019), [arXiv:1910.12085](#).
- [52] C. Huang, M. Newman, and M. Szegedy, Explicit lower bounds on strong quantum simulation, *IEEE Transactions on Information Theory* **66**, 5585 (2020), [arXiv:1804.10368](#).
- [53] K. De Raedt, K. Michielsen, H. De Raedt, B. Trieu, G. Arnold, M. Richter, T. Lippert, H. Watanabe, and N. Ito, Massively parallel quantum computer simulator, *Computer Physics Communications* **176**, 121 (2007), [arXiv:quant-ph/0608239](#).
- [54] R. Raussendorf and J. Harrington, Fault-Tolerant Quantum Computation with High Threshold in Two Dimensions, *Phys. Rev. Lett.* **98**, 190504 (2007), [arXiv:quant-ph/0610082](#).
- [55] R. Raussendorf, J. Harrington, and K. Goyal, Topological fault-tolerance in cluster state quantum computation, *New Journal of Physics* **9**, 199 (2007), [arXiv:quant-ph/0703143](#).
- [56] The average fidelity of a m -qubit noise channel \mathcal{N} acting on a normalized random n -qubit state is
- $$f^{(n)} = \mathbb{E}_{\psi \in \mathbb{C}^{2^n}} \langle \psi | \mathcal{N}(|\psi\rangle\langle\psi|) | \psi \rangle = \frac{f + 2^{-n}}{1 + 2^{-n}}$$
- f is the average entanglement fidelity [77, 78] and the $n \rightarrow \infty$ limit of $f^{(n)}$:
- $$f = \lim_{n \rightarrow \infty} f^{(n)} = 2^{-2m} \sum_k \text{tr}(E_k) \text{tr}(E_k^\dagger)$$
- where $\mathcal{N}(\rho) = \sum_k E_k \rho E_k^\dagger$ is the Kraus decomposition of \mathcal{N} . The average gate fidelity is often defined as $f^{(m)}$.
- [57] D. Gottesman, An Introduction to Quantum Error Correction and Fault-Tolerant Quantum Computation, (2009), [arXiv:0904.2557](#).
- [58] M. Sarovar, T. Proctor, K. Rudinger, K. Young, E. Nielsen, and R. Blume-Kohout, Detecting crosstalk errors in quantum information processors, *Quantum* **4**, 321 (2020), [arXiv:1908.09855](#).
- [59] M. McEwen, L. Faoro, K. Arya, A. Dunsworth, T. Huang, S. Kim, B. Burkett, A. Fowler, F. Arute, J. C. Bardin, A. Bengtsson, A. Biles, B. B. Buckley, N. Bushnell, Z. Chen, R. Collins, S. Demura, A. R. Derk, C. Erickson, M. Giustina, S. D. Harrington, S. Hong, E. Jeffrey, J. Kelly, P. V. Klimov, F. Kostritsa, P. Laptev, A. Locharla, X. Mi, K. C. Miao, S. Montazeri, J. Mutus, O. Naaman, M. Neeley, C. Neill, A. Opremcak, C. Quintana, N. Redd, P. Roushan, D. Sank, K. J. Satzinger, V. Shvarts, T. White, Z. J. Yao, P. Yeh, J. Yoo, Y. Chen, V. Smelyanskiy, J. M. Martinis, H. Neven, A. Megrant, L. Ioffe, and R. Barends, Resolving catastrophic error bursts from cosmic rays in large arrays of superconducting qubits, (2021), [arXiv:2104.05219](#).
- [60] The diagonal terms are bounded by $|\chi_{\alpha\alpha}^{(u)}| \leq 1 - f_u$ for $\alpha \neq \mathbf{0}$ since \mathcal{N}_u is trace preserving: $\text{tr} \mathcal{N}_u(\rho) = \text{tr} \rho$. The absolute value of the off-diagonal $\alpha \neq \beta$ terms are then upper bounded by $|\chi_{\alpha\beta}^{(u)}| \leq \sqrt{|\chi_{\alpha\alpha}^{(u)}| |\chi_{\beta\beta}^{(u)}|} \leq \sqrt{f_u (1 - f_u)}$ since $\chi^{(u)}$ is a positive semi-definite matrix.
- [61] A. Nahum, S. Vijay, and J. Haah, Operator Spreading in Random Unitary Circuits, *Physical Review X* **8**, 021014 (2018), [arXiv:1705.08975](#).
- [62] C. W. von Keyserlingk, T. Rakovszky, F. Pollmann, and S. L. Sondhi, Operator Hydrodynamics, OTOCs, and Entanglement Growth in Systems without Conservation Laws, *Physical Review X* **8**, 021013 (2018), [arXiv:1705.08910](#).
- [63] D. A. Roberts, D. Stanford, and L. Susskind, Localized shocks, *Journal of High Energy Physics* **2015**, 51 (2015), [arXiv:1409.8180](#).
- [64] A. Harrow and S. Mehraban, Approximate unitary t -designs by short random quantum circuits using nearest-neighbor and long-range gates, (2018), [arXiv:1809.06957](#).
- [65] After spreading out, a single Pauli error results in a fidelity $\sim \mathbb{E}_\psi |\langle \psi | \sigma | \psi \rangle|^2 = (2^n + 1)^{-1}$, where ψ and U are random n -qubit states and unitaries and σ is a Pauli operator.
- [66] U. Schollwöck, The density-matrix renormalization group in the age of matrix product states, *Annals of Physics* **326**, 96 (2011), [arXiv:1008.3477](#).
- [67] E. M. Stoudenmire and S. R. White, Real-space parallel density matrix renormalization group, *Phys. Rev. B* **87**, 155137 (2013), [arXiv:1301.3494](#).
- [68] J. Eisert, Entanglement and tensor network states,

- (2013), [arXiv:1308.3318](#).
- [69] A. Gheorghiu, T. Kapourniotis, and E. Kashefi, Verification of quantum computation: An overview of existing approaches, *Theory of Computing Systems* **63**, 715–808 (2019), [arXiv:1709.06984](#).
 - [70] J. Eisert, D. Hangleiter, N. Walk, I. Roth, D. Markham, R. Parekh, U. Chabaud, and E. Kashefi, Quantum certification and benchmarking, *Nature Reviews Physics* **2**, 382 (2020), [arXiv:1910.06343](#).
 - [71] D. Aharonov and U. Vazirani, Is Quantum Mechanics Falsifiable? A computational perspective on the foundations of Quantum Mechanics, (2012), [arXiv:1206.3686](#).
 - [72] P. Shor, Algorithms for quantum computation: discrete logarithms and factoring, in *Proceedings 35th Annual Symposium on Foundations of Computer Science* (1994) pp. 124–134.
 - [73] C. Gidney and M. Ekerå, How to factor 2048 bit RSA integers in 8 hours using 20 million noisy qubits, *Quantum* **5**, 433 (2021), [arXiv:1905.09749](#).
 - [74] J. M. Epstein, A. W. Cross, E. Magesan, and J. M. Gambetta, Investigating the limits of randomized benchmarking protocols, *Phys. Rev. A* **89**, 062321 (2014), [arXiv:1308.2928](#).
 - [75] H. Ball, T. M. Stace, S. T. Flammia, and M. J. Biercuk, Effect of noise correlations on randomized benchmarking, *Phys. Rev. A* **93**, 022303 (2016), [arXiv:1504.05307](#).
 - [76] S. Aaronson, Quantum Computing, Postselection, and Probabilistic Polynomial-Time, (2004), [arXiv:quant-ph/0412187](#).
 - [77] M. A. Nielsen, The entanglement fidelity and quantum error correction, (1996), [arXiv:quant-ph/9606012](#).
 - [78] B. Schumacher, Sending quantum entanglement through noisy channels, (1996), [arXiv:quant-ph/9604023](#).
 - [79] T. Proctor, M. Revelle, E. Nielsen, K. Rudinger, D. Lobser, P. Maunz, R. Blume-Kohout, and K. Young, Detecting and tracking drift in quantum information processors, *Nature Communications* **11**, 5396 (2020), [arXiv:1907.13608](#).
 - [80] A. Erhard, J. J. Wallman, L. Postler, M. Meth, R. Stricker, E. A. Martinez, P. Schindler, T. Monz, J. Emerson, and R. Blatt, Characterizing large-scale quantum computers via cycle benchmarking, *Nature Communications* **10**, 5347 (2019), [arXiv:1902.08543](#).
 - [81] G. Evenbly, Gauge fixing, canonical forms, and optimal truncations in tensor networks with closed loops, *Phys. Rev. B* **98**, 085155 (2018), [arXiv:1801.05390](#).
 - [82] J. Haegeman, C. Lubich, I. Oseledets, B. Vandereycken, and F. Verstraete, Unifying time evolution and optimization with matrix product states, *Phys. Rev. B* **94**, 165116 (2016), [arXiv:1408.5056](#).
 - [83] M. Lubasch, J. I. Cirac, and M.-C. Bañuls, Algorithms for finite projected entangled pair states, *Phys. Rev. B* **90**, 064425 (2014), [arXiv:1405.3259](#).
 - [84] L. Vanderstraeten, J. Haegeman, P. Corboz, and F. Verstraete, Gradient methods for variational optimization of projected entangled-pair states, *Phys. Rev. B* **94**, 155123 (2016), [arXiv:1606.09170](#).
 - [85] J. S. Bell, On the einstein podolsky rosen paradox, *Physics Physique Fizika* **1**, 195 (1964).
 - [86] D. M. Greenberger, M. A. Horne, A. Shimony, and A. Zeilinger, Bell’s theorem without inequalities, *American Journal of Physics* **58**, 1131 (1990).
 - [87] N. D. Mermin, Quantum mysteries revisited, *American Journal of Physics* **58**, 731 (1990).
 - [88] J.-W. Pan, D. Bouwmeester, M. Daniell, H. Weinfurter, and A. Zeilinger, Experimental test of quantum nonlocality in three-photon Greenberger-Horne-Zeilinger entanglement, *Nature (London)* **403**, 515 (2000).
 - [89] S. Hossenfelder and T. Palmer, Rethinking Superdeterminism, *Frontiers in Physics* **8**, 139 (2020), [arXiv:1912.06462](#).
 - [90] J.-Å. Larsson, Loopholes in Bell inequality tests of local realism, *Journal of Physics A Mathematical General* **47**, 424003 (2014), [arXiv:1407.0363](#).
 - [91] S. Aaronson, Quantum computing and hidden variables, *Phys. Rev. A* **71**, 032325 (2005), [arXiv:quant-ph/0408035](#).
 - [92] I. Cirac, D. Perez-Garcia, N. Schuch, and F. Verstraete, Matrix Product States and Projected Entangled Pair States: Concepts, Symmetries, and Theorems, (2020), [arXiv:2011.12127](#).

Appendix A: Exponential Fidelity Decay via 2-design Twirling

Given a gate independent noise assumption and 2-design⁶ approximation, we can generalize the randomized benchmarking 2-design twirling argument [39] to our protocol. Similar to the main texts, we find that quantum mechanics predicts an exponential fidelity decay [Eq. (6)].

We assume that the noise is gate and time independent, but it may depend on the position of the 2-qubit gate. Therefore, in the notation of Sec. III, the noise channels are assumed to be the same for different 2-qubit gates $u_{t,i}$ and $u_{t',i}$ acting on the same pair of qubits labeled by i : $\mathcal{N}_{u_{t,i}} = \mathcal{N}_{u_{t',i}}$. However, we can allow the noise for the forward and backward circuits to be different. As is also the case in the main text, it is not essential to assume that the noise only comes from 2-qubit error channels.

We also approximate each layer of 2-qubit gates U_t as a 2-design. Formally, this approximation is not justified since an approximate 2-design requires a $O(n^{1/D})$ -depth D -dimensional circuit [64]. However, this approximation might be better than expected if we can instead think of it as only approximating the composition of $O(n^{1/D})$ layers of gates as a 2-design. We do not consider this possibility here since it would complicate the definition of the noise channel \mathcal{N} below.

To simplify the notation, we rewrite the Markovian fidelity Eq. (3) from the main text as

$$F_d = \mathbb{E}_{U_1, \dots, U_d} \text{tr}(\rho'_d \rho_d) \quad (\text{A1})$$

where

$$\begin{aligned} \rho'_d &\equiv (\Phi_{U_d}^\dagger \circ \dots \circ \Phi_{U_1}^\dagger)(\rho^{\text{fin}}) \\ \rho_d &\equiv (\Phi_{U_d} \circ \dots \circ \Phi_{U_1})(\rho^{\text{init}}) \end{aligned} \quad (\text{A2})$$

implicitly depend on U_1, \dots, U_d , and Φ^\dagger is defined such that $\text{tr}[\Phi^\dagger(\rho') \rho] = \text{tr}[\rho' \Phi(\rho)]$. Below we recursively integrate out one U_t at a time by approximating each U_t as an arbitrary Haar random unitary (or a unitary 2-design) on n qubits:

$$F_d = \mathbb{E}_{U_1, \dots, U_d} \text{tr} \left[\mathcal{N}_d'^\dagger(\rho'_{d-1}) U_d^\dagger \mathcal{N}_d(U_d \rho_{d-1} U_d^\dagger) U_d \right] \quad (\text{A3})$$

$$\sim \frac{\hat{F}_d - 2^{-2n}}{1 - 2^{-2n}} \mathbb{E}_{U_1, \dots, U_{d-1}} \text{tr} \left[\mathcal{N}_d'^\dagger(\rho'_{d-1}) \rho_{d-1} \right] + (1 - \hat{F}_d) \frac{2^{-n}}{1 - 2^{-2n}} \text{tr} \mathcal{N}_d'^\dagger(\rho'_{d-1}) \quad (\text{A4})$$

$$\sim \left(\prod_{t=d'+1}^d \frac{\hat{F}_t - 2^{-2n}}{1 - 2^{-2n}} \right) \mathbb{E}_{U_1, \dots, U_{d'}} \text{tr} \left[\mathcal{N}_{d'}'^\dagger(\rho'_{d'-1}) U_{d'}^\dagger (\mathcal{N}_{d'+1}' \circ \mathcal{N}_{d'}) (U_{d'} \rho_{d'-1} U_{d'}^\dagger) U_{d'} \right] \quad (\text{A5})$$

$$\begin{aligned} &+ \sum_{t=d'+1}^d (1 - \hat{F}_t) \frac{2^{-n}}{1 - 2^{-2n}} \text{tr} \mathcal{N}_t'^\dagger(\rho'_{t-1}) \\ &\sim \left(\prod_{t=1}^d \frac{\hat{F}_t - 2^{-2n}}{1 - 2^{-2n}} \right) \text{tr} \left[\mathcal{N}_1'^\dagger(\rho^{\text{fin}}) \rho^{\text{init}} \right] + \sum_{t=1}^d (1 - \hat{F}_t) \frac{2^{-n}}{1 - 2^{-2n}} \text{tr} \mathcal{N}_t'^\dagger(\rho'_{t-1}) \end{aligned} \quad (\text{A6})$$

$$= \text{tr} \left[\mathcal{N}_1'^\dagger(\rho^{\text{fin}}) \rho^{\text{init}} \right] \prod_{t=1}^d \hat{F}_t + O(2^{-n}) \quad (\text{A7})$$

\mathcal{N}_t and \mathcal{N}_t' are gate-independent noise channels of the forward and backward circuits: $\Phi_{U_t}(\rho) = \mathcal{N}_t(U_t \rho U_t^\dagger)$ and $\Phi_{U_t}^\dagger(\rho) = \mathcal{N}_t'(U_t^\dagger \rho U_t)$. In the last line, we drop very small $O(2^{-n})$ terms. \hat{F}_t is the entanglement fidelity of $\mathcal{N}_{t+1}' \circ \mathcal{N}_t$ for $t = 1, \dots, d-1$, while \hat{F}_d is just the entanglement fidelity of \mathcal{N}_d :

$$\begin{aligned} \hat{F}_t &= 2^{-2n} \text{tr}(\mathcal{N}_{t+1}' \circ \mathcal{N}_t) & \hat{F}_d &= 2^{-2n} \text{tr} \mathcal{N}_t \\ &= 2^{-2n} \sum_{k', k} \left| \text{tr} \left(E_{k'}'^{(t+1)} E_k^{(t)} \right) \right|^2 & &= 2^{-2n} \sum_k \left| \text{tr} E_k^{(t)} \right|^2 \end{aligned} \quad (\text{A8})$$

⁶ We thank Alex Dalzell for pointing out that a 2-design approximation is sufficient, rather than a 4-design.

$E_k^{(t)}$ and $E_{k'}^{(t)}$ are Kraus operators of \mathcal{N}_t and \mathcal{N}'_t ; *i.e.* $\mathcal{N}_t(\rho) = \sum_k E_k^{(t)} \rho E_k^{(t)\dagger}$ and $\mathcal{N}'_t(\rho) = \sum_{k'} E_{k'}^{(t)} \rho E_{k'}^{(t)\dagger}$. Note that $\hat{F}_t = \hat{F}_{t+p}$ has periodicity p since the circuit geometry is assumed to have periodicity p .

The entanglement fidelity of the composition $\mathcal{N}'_{t+1} \circ \mathcal{N}_t$ appears in Eq. (A8) because coherent errors can cancel out. For example, if $\mathcal{N}_t(\rho) = V \rho V^\dagger$ and $\mathcal{N}'_{t+1}(\rho) = V^\dagger \rho V$ for some unitary V , then the fidelity F_d would not depend on the coherent error V . This subtlety does not occur in randomized benchmarking [38–40] because randomized benchmarking uses a compactified inverse circuit.

Eq. (A7) is an exponential fidelity decay $F_d \sim \tilde{F}_0 e^{-\lambda d}$ with parameters

$$\begin{aligned} \tilde{F}_0 &\approx \text{tr} \left[\mathcal{N}'_1(\rho^{\text{fin}}) \rho^{\text{init}} \right] \frac{\text{tr} \mathcal{N}_p}{\text{tr}(\mathcal{N}'_{p+1} \circ \mathcal{N}_p)} \\ \lambda &\approx -\frac{1}{p} \log \prod_{t=1}^p \hat{F}_t \end{aligned} \quad (\text{A9})$$

when d is an integer multiple of the period p .

Eq. (A9) differs from Eq. (7) in the main text for two reasons: Eq. (7) neglected the fact that coherent errors in $\mathcal{N}'_{t+1} \circ \mathcal{N}_t$ can cancel out, while Eq. (A9) assumes that errors are gate-independent. Unfortunately, the decay rate λ in Eq. (A9) can not be written in terms of a product of 2-qubit gate fidelities [as in Eq. (7)] because $\mathcal{N}'_{t+1} \circ \mathcal{N}_t$ in the definition of \hat{F}_t involves two circuit layers with different positions of the 2-qubit gates. If we were to make the rough approximation $2^{-2n} \text{tr}(\mathcal{N}'_{t+1} \circ \mathcal{N}_t) \rightarrow 2^{-4n} \text{tr} \mathcal{N}'_{t+1} \text{tr} \mathcal{N}_t$, then λ in Eq. (A9) would simplify to Eq. (7).

Appendix B: Numerical Simulations

In Fig. 3 we showed a simulation for a 5×5 grid of $n = 25$ qubits using roughly Sycamore/Zuchongzhi-like [9–11] gates with gate-dependent errors. Appendices B1 and B2 specify the gate and noise models that we used. Appendix B3 defines an optimized basis of Kraus operators that we used to minimize the amount of statistical sampling error. All plots in the main text have statistical errors that are too small to be seen. Appendix B4 specifies details used to produce the MPS data in Fig. 4.

In Fig. 5, we show a more detailed version of Fig. 3 showing a larger max circuit depth d_{max} . At large depth, the fidelity F_d saturates to 2^{-n} , which will be too small to be experimentally observable for large $n \gtrsim 50$. Fig. 5b shows the residual errors to the exponential decay fit. The $\log(F_d) - \text{fit}$ residuals are dominated by the 2^{-n} saturation at large depth. After subtracting off 2^{-n} , we see that $F_d - 2^{-n}$ agrees with an exponential decay up to statistical errors. The statistical errors of $F_d - 2^{-n}$ become very large once the fidelity decays to 2^{-n} due to the 2^{-n} subtraction.

To investigate the residuals with less statistical error, we also ran a simulation with less qubits (for which we can run significantly more Monte Carlo samples). Fig. 6 is similar to Fig. 5, but for a simulation of a 3×3 grid of $n = 9$ qubits and a smaller average gate entanglement fidelity $f \approx 0.987$ (instead of $f \approx 0.993$). In Fig. 6b, we see that residual errors to an exponential fit are very small when $F_d \gg 2^{-n}$.

1. Gate Model

In our numerical simulations, we use gates that are somewhat similar to the Sycamore/Zuchongzhi gates [9–11]. The gates are applied in the order shown in Fig. 5c.

Each 2-qubit gate $u_{t,i}$ is an iSWAP gate (rather than Sycamore/Zuchongzhi iSWAP-like gates [9–11])

$$U_{\text{iSWAP}} = \begin{pmatrix} 1 & 0 & 0 & 0 \\ 0 & 0 & -i & 0 \\ 0 & -i & 0 & 0 \\ 0 & 0 & 0 & 1 \end{pmatrix} \quad (\text{B1})$$

that is preceded by a pair of randomly chosen 1-qubit gates (\sqrt{X} , \sqrt{Y} , or \sqrt{W}) on two qubits, where $W = \frac{1}{\sqrt{2}}(X + Y)$. Using $U_{\text{iSWAP}}^\dagger = U_{\text{iSWAP}}(Z \otimes Z)$, we decompose the inverse gate $u_{t,i}^\dagger$ as an iSWAP gate followed by a $\sqrt{X}^\dagger Z$, $\sqrt{Y}^\dagger Z$, or $\sqrt{W}^\dagger Z$ gate on each of the two qubits.

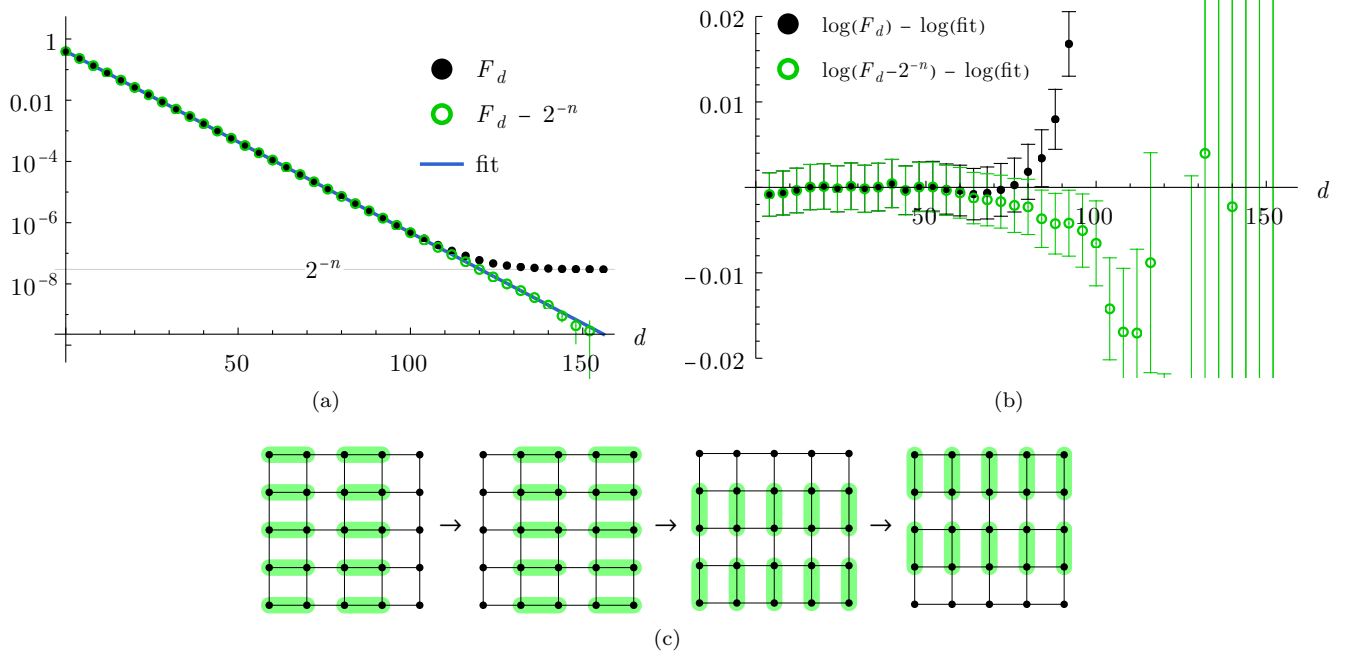


FIG. 5. **(a)** The same simulation data (black dots) as Fig. 3 (but for larger max depth d_{\max}) showing the quantum mechanics prediction of the exponential fidelity F_d decay for a 5×5 grid of $n = 25$ noisy qubits. The fidelity F_d saturates to 2^{-n} at large circuit depth d . Subtracting 2^{-n} from F_d (green circles) leads to a continued exponential decay (at least until our simulation data becomes dominated by statistical errors). Also shown is a fit (blue line) to an exponential decay. **(b)** With 2^{-n} subtracted, the fit residuals are dominated by statistical errors for our simulation of 10,000 Monte Carlo samples. Error bars denote one standard deviation (*i.e.* 68% confidence intervals). **(c)** The period $p = 4$ ordering of 2-qubit gates (green) applied to the 5×5 array of qubits.

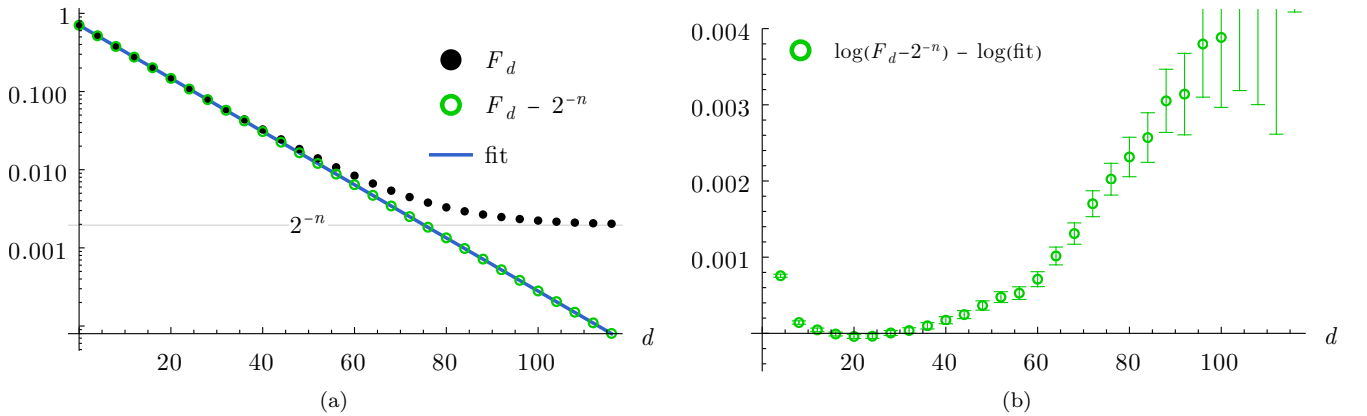


FIG. 6. Same as Fig. 5, but for a 3×3 grid of $n = 9$ qubits, for which we obtained 8×10^7 Monte Carlo samples. Panel (b) shows that the residual errors of $F_d - 2^{-n}$ to an exponential fit are very small.

2. Noise Model

In our numerical simulations, we use a generic error model with gate and position dependent errors. Each iSWAP gate for each pair of qubits (labeled by i) has a unique noise channel. And for each of the n qubits, we apply a unique noise channel for each of six the 1-qubit gates (\sqrt{X} , \sqrt{Y} , \sqrt{W} , $\sqrt{X}^\dagger Z$, $\sqrt{Y}^\dagger Z$, and $\sqrt{W}^\dagger Z$). Each noise channel is generated randomly. None of our plots appear to differ qualitatively for different random instances of gate error channels.

One way to generate a random noise channel on a d -dimensional Hilbert space is to choose a set of m Kraus operators as a Haar random $md \times d$ semi-unitary matrix $E_{ka,b}$ (i.e. $\sum_{ka} E_{ka,b'}^* E_{ka,b} = \delta_{b',b}$). Then the noise channel is

$$\mathcal{N}_m(\rho) \stackrel{\text{rand}}{=} \sum_{k=1}^m E_k \rho E_k^\dagger \quad (\text{B2})$$

In order to cover the set of all noise channels, one must choose $m = d^2$. However, for $d = 4$ or larger, this leads to a distribution of noise channels that is strongly concentrated near the depolarizing channel. In order to obtain a broader but still generic distribution of noise channels, we generate each random noise channel as an average of the above random noise channel for $m = 1, 2, \dots, d^2$:

$$\mathcal{N}_{\text{rand}}(\rho) \stackrel{\text{rand}}{=} d^{-2} \sum_{m=1}^{d^2} \mathcal{N}_m(\rho) \quad (\text{B3})$$

We also apply a randomly-chosen coherent error for each gate. For a d -dimensional Hilbert space, we generate coherent error channels using a random unitary that is generated by

$$U_p \stackrel{\text{rand}}{=} e^{i\sqrt{\frac{p}{d^2-1}} H_{\text{rand}}^{\text{Gauss}}} \quad (\text{B4})$$

where $H_{\text{rand}}^{\text{Gauss}}$ is a complex standard Gaussian random matrix and p tunes the infidelity.

Each noise channel is then generated via

$$\mathcal{N}_p(\rho) \stackrel{\text{rand}}{=} U_{p''/2} \left[\left(1 - \frac{p'}{2}\right) \rho + \frac{p'}{2} \mathcal{N}_{\text{rand}}(\rho) \right] U_{p''/2}^\dagger \quad (\text{B5})$$

where p' and p'' are randomly chosen between $p/\sqrt{2}$ and $\sqrt{2}p$. The entanglement fidelity of \mathcal{N}_p is roughly $1 - p$.

We randomly generated the 2-qubit iSWAP noise channel using \mathcal{N}_{p_2} , while the 1-qubit noise channels were randomly generated using \mathcal{N}_{p_1} , with $p_1 = 0.1p_2$. For Figs. 3, 4, and 5, we used $p_2 = 0.005$. For Fig. 6, we used $p_2 = 0.01$.

3. Simulation Algorithm Details

We simulate the fidelity in Eq. (3) by Monte Carlo (MC) sampling the density matrices and quantum channels such that only two wavefunctions are stored in memory: one from ρ^{init} and the other from ρ^{fin} . To reduce the amount of statistical error, we sample the density matrices and quantum channels such that each MC sample has the same average entanglement fidelity.

That is, ρ^{init} and ρ^{fin} are uniformly sampled from unnormalized wavefunctions $|\psi_k^{\text{init}}\rangle$ and $|\psi_k^{\text{fin}}\rangle$:

$$\begin{aligned} \rho^{\text{init}} &= \mathbb{E}_k |\psi_k^{\text{init}}\rangle \langle \psi_k^{\text{init}}| \\ \rho^{\text{fin}} &= \mathbb{E}_k |\psi_k^{\text{fin}}\rangle \langle \psi_k^{\text{fin}}| \end{aligned} \quad (\text{B6})$$

which are chosen to have the same fidelity:

$$\begin{aligned} \langle 0 | \psi_k^{\text{init}} \rangle &= \langle 0 | \psi_{k'}^{\text{init}} \rangle \\ \langle 0 | \psi_k^{\text{fin}} \rangle &= \langle 0 | \psi_{k'}^{\text{fin}} \rangle \end{aligned} \quad (\text{B7})$$

In Eq. (B6), $\mathbb{E}_k \equiv n_k^{-1} \sum_k$ denotes an expectation value over n_k uniformly random k . Similarly, the quantum channels Φ_u are rewritten using a Kraus decomposition

$$\Phi_u(\rho) = \mathbb{E}_k E_k^{(u)} \rho E_k^{(u)\dagger} \quad (\text{B8})$$

(with nonstandard normalization due to the \mathbb{E}_k) such that each Kraus operator has the same trace:

$$\text{tr } E_k^{(u)} = \text{tr } E_{k'}^{(u)} \quad (\text{B9})$$

This implies that each Kraus operator has the same entanglement fidelity as Φ_u : $f_u = 2^{-2m} \text{tr } E_k^{(u)} \text{tr } E_k^{(u)\dagger}$ where $E_k^{(u)}$ is a $2^m \times 2^m$ matrix. With this optimization, for a given sequence of unitaries U_1, \dots, U_d , each MC sample has the approximately the same fidelity, which leads to a significant reduction in MC statistical error.

We only require that these special wavefunctions and Kraus operators obey linear constraints [Eq. (B7) and (B9)]. They can therefore be obtained from another decomposition (*e.g.* an eigendecomposition), $\rho = \mathbb{E}_{\tilde{k}} |\tilde{\psi}_{\tilde{k}}\rangle \langle \tilde{\psi}_{\tilde{k}}|$ or $\Phi(\rho) = \mathbb{E}_{\tilde{k}} \tilde{E}_{\tilde{k}} \rho \tilde{E}_{\tilde{k}}^\dagger$, via a unitary transformation $V_{k,\tilde{k}}$ that rotates the vector $v_{\tilde{k}} = \langle 0 | \tilde{\psi}_{\tilde{k}} \rangle$ (or $v_{\tilde{k}} = \text{tr } \tilde{E}_{\tilde{k}}$) to $\sum_{\tilde{k}} V_{k,\tilde{k}} v_{\tilde{k}} = \sqrt{f}$ for some constant fidelity $f > 0$. That is, $|\psi_k\rangle = V_{k,\tilde{k}} |\tilde{\psi}_{\tilde{k}}\rangle$ and $E_k = V_{k,\tilde{k}} \tilde{E}_{\tilde{k}}$.

Each MC sample for a sequence of fidelities F_d with $d = 0, \dots, d_{\max}$ is then obtained as follows:

1. sample initial forward circuit wavefunction: $|\psi\rangle \leftarrow |\psi_k^{\text{init}}\rangle$ for uniformly random k
2. sample final backward circuit wavefunction: $|\psi'\rangle \leftarrow |\psi_k^{\text{fin}}\rangle$ for uniformly random k
3. foreach circuit depth $d = 1, \dots, d_{\max}$:
 - (a) foreach 2-qubit gate position i :
 - i. randomly sample an allowed gate: $u_{d,i}$
 - ii. apply random Kraus operator for forward gate: $|\psi\rangle \leftarrow E_k^{(u_{d,i})} |\psi\rangle$ for uniformly random k
 - iii. apply random Kraus operator for backward gate: $|\psi'\rangle \leftarrow E_k^{(u_{d,i}^\dagger)^\dagger} |\psi'\rangle$ for uniformly random k
 - (b) obtain fidelity sample: $F_d \leftarrow |\langle \psi' | \psi \rangle|^2$

4. MPS Simulation

In Fig. 4, we showed a MPS simulation of our protocol with noisy gates for a chain of 24 qubits. We used the same noise and gate models and sampling algorithm as in Fig. 3, *i.e.* the models in Appendices B1 and B2 and algorithm in Appendix B3

Random gates, SPAM errors, and random Kraus operators are randomly sampled as described in Appendix B3. However, a subtlety results from the fact that the MPS simulation introduces non-linear truncation errors. When there is no truncation error, as in the quantum mechanics prediction (blue in Fig. 4), then changing the Kraus operator basis $E_k \rightarrow V_{k,k'} E_{k'}$ does not affect the fidelity. But when there is truncation error, the choice of Kraus operator basis will affect the simulation result. Typically, Kraus operators that are more like measurement operators will reduce the amount of entanglement, which decreases the amount of truncation error in later truncation steps. Alternatively, Kraus operators that are closer to unitary operators typically result in a larger truncation error. We use the Kraus basis defined in Appendix B3 or the MPS simulation, which is a nice choice because all of the Kraus operators behave similarly with similar fidelity.

Appendix C: Drift

While iterating our protocol many times (*e.g.* over the course of hours) to obtain a large number of samples, slow temperature fluctuations (and other causes) can result in miscalibrations (and other complications) that slowly drift [79] over time. As a result, the effective error channel of each gate can change over time, resulting in slowly-varying gate fidelities [80] for different samples. To mitigate issues resulting from drift, our protocol samples a random circuit depth d for each sample. If circuit depth was instead sampled in increasing order, then drift could potentially cause the gate fidelity to decrease over time, which could then lead to a fidelity F_d decay that could be mistaken for the EmQM signature. By randomly sampling circuit depth, we can show that the effect of slow temporal drift can only cause the exponential fidelity F_d decay rate to slightly decrease with circuit depth d , rather than increase as for EmQM. This occurs because if the drift occurs much slower than the time scale to sample all circuit depths, then for larger depth, the fidelity F_d is dominated by rare samples with rare but higher gate fidelities (due to rare drifts),

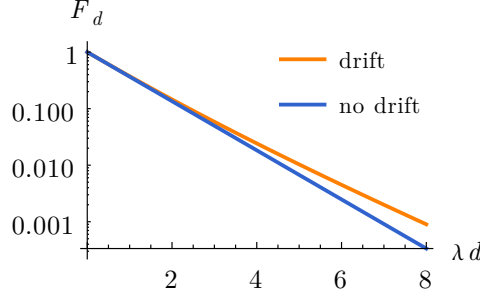


FIG. 7. An exponential fidelity decay $F_d = e^{-\lambda d}$ without drift (blue) vs a fidelity decay with drift (orange) [Eq. (C2) with $\lambda_1 = \frac{2}{3}\lambda$ and $\lambda_2 = \frac{4}{3}\lambda$]. Drift only causes the fidelity to decay slightly slower at larger depth, which can not be mistaken for the EmQM signature [shown in Fig. 2].

while at smaller depth the fidelity is dominated by typical gate fidelities. As such, the effects of drift are unlikely to be confused with the EmQM signature.

To see this more explicitly, we can consider the following toy model. Assume that quantum mechanics is correct and suppose that temporal drifts occur over a time scale that is much longer than the time it takes to run a single sample in our protocol. Then suppose that due to drift, the probability that a sample measures a zero state is the following time-dependent fidelity:

$$F_d(t) = e^{-\lambda(t)d} \quad (\text{C1})$$

Similar to Eq. (2), the fidelity decays exponentially with circuit depth d (although we neglect SPAM errors, *i.e.* the \tilde{F}_0 factor, for simplicity). However, the fidelity also depends on time since the exponential decay rate $\lambda(t)$ is time-dependent due to slow time-dependent drifts.

To gain intuition, suppose that the fidelity decay rate $\lambda(t)$ drifts between λ_1 and λ_2 with a uniform probability distribution in-between. Then the average probability that a sample measures a zero state is the average fidelity:

$$\begin{aligned} F_d &= \frac{1}{\lambda_2 - \lambda_1} \int_{\lambda_1}^{\lambda_2} e^{-\lambda d} d\lambda \\ &= \frac{1}{d} \frac{e^{-\lambda_1 d} - e^{-\lambda_2 d}}{\lambda_2 - \lambda_1} \end{aligned} \quad (\text{C2})$$

See Fig. 7 for an example plot. At small depth, $F_d \approx e^{-\lambda d}$ where $\lambda = \frac{1}{2}(\lambda_1 + \lambda_2)$, while at large depth $F_d \approx (\lambda_2 - \lambda_1)^{-1} \frac{1}{d} e^{-\lambda_1 d}$. Thus the fidelity decays slower at larger depth (in contrast to the EmQM signature) since $\lambda_1 < \lambda$.

Now consider a general probability distribution $P(\lambda)$ of fidelity decay rates $\lambda(t)$ after time averaging. Then the fidelity is $F_d = \int_{\lambda} e^{-\lambda d}$ where $\int_{\lambda} f(\lambda) \equiv \int_0^{\infty} f(\lambda) P(\lambda) d\lambda$ averages over the different decay rates. In this general setting, we can also show that the fidelity decays slower at larger depth. The exponential decay rate near a given depth is the average of $\lambda(t)$:

$$-\partial_d \log F_d = \langle \lambda \rangle_d \quad \text{where} \quad \langle f(\lambda) \rangle_d \equiv \frac{\int_{\lambda} f(\lambda) e^{-\lambda d}}{\int_{\lambda} e^{-\lambda d}} \quad (\text{C3})$$

The slope of the curve $\log F_d$ is thus $-\langle \lambda \rangle_d$. The derivative of this slope is then the variance of $\lambda(t)$:

$$-\partial_d \langle \lambda \rangle_d = \langle (\lambda - \langle \lambda \rangle_d)^2 \rangle_d \quad (\text{C4})$$

Since the above variance is always positive, the derivative of the slope of $\log F_d$ vs d is always positive. This implies that the fidelity decays slower at larger depth than slower depth, which is opposite of the EmQM signature.

Appendix D: MPS

In Sec. IV, we considered the time evolution of matrix product states (MPS) [66] with fixed bond dimension as an (incomplete) toy model of emergent quantum mechanics (EmQM) in one spatial dimension. And in Appendix E 2 we explain how and why tensor networks are not ruled out by Bell experiments. However, we do not consider MPS to be a legitimate model of EmQM because it is currently not known how (or if it is possible) to generalize MPS algorithms to a three-dimensional local classical theory that could be compatible with previous experiments. We elaborate on this point below.

One of the hallmarks of MPS is the canonical form, which allows one to calculate the expectation value of a local operator near some position x in terms of only the tensors near x . When generalizing MPS to higher dimensions, this sense of canonical form can either be retained, as is done for isometric tensor networks [23–25]; or the canonical form can be dropped, as is done for projected entangled pair states (PEPS) [22]; or the canonical form can be replaced with something new (but less constraining), such as a weighted trace gauge (WTG) [81].

When the canonical form is retained [23–25], a local update algorithm to time evolve the tensor network is known [23]. However, the algorithm does not quite yet yield a local classical theory since the update algorithm has to iteratively sweep across the tensor network. This is similar to many MPS algorithms, such as TDVP [82], which time evolve a length- L chain by performing a forward sweep to update the tensors at sites i and $i+1$ for $i = 1, 2, \dots, L-1$, followed by a backward sweep with $i = L-1, L-2, \dots, 1$. It would be incredibly unnatural if the time evolution of the universe sweeps across space in this serial (rather than parallel) manner. Therefore, we expect an EmQM theory to have the form of a local classical theory: *i.e.* a (possibly continuous) cellular automaton for which the local updates are performed in parallel for all sites at once. Nevertheless, we expect that it is possible to parallelize the time-evolving isometric tensor network algorithm [23] into a continuous cellular automaton, *e.g.* by using ideas from Ref. [67].

However, there is a more severe issue that is also shared with MPS: between certain pairs of well-separated spatial disks of radius ℓ , isometric tensor networks [23] and canonical PEPS [24, 25] can only represent wavefunctions that have a bounded amount of entanglement between the two regions. In particular, the mutual information I between certain pairs of regions is bounded by the log of the bond dimension χ : $I < \log \chi$. Even a large bond dimension $\chi = 1024$ is only large enough to encode 10 bell pairs between the two regions. Unless χ is extraordinarily large, this is incompatible with many experiments, including the recent quantum advantage experiments [9–12].⁷

An EmQM theory should allow the mutual information to diverge with the length scale ℓ , so that quantum mechanics with highly-entangled quantum states can emerge in the large length limit $\ell \rightarrow \infty$.

On the other hand, PEPS do appear to be possibly powerful enough to represent wavefunctions that are sufficiently entangled to be compatible with current experimental observations. For example, the mutual information bound for PEPS diverges linearly with the length scale: $I < O(\ell \log \chi)$. Furthermore, due to their unconstrained nature, unitary circuits can easily be embedded into a PEPS in order to represent high-complexity wavefunctions. This is especially true if the PEPS exists in extra spatial dimensions and/or if physical qubits are separated by large distances in the lattice of tensors, as in Fig. 8.

However, we are not aware of any time-evolving PEPS algorithms that could be written as a local classical theory. For example, PEPS update algorithms typically require calculating environment tensors, which involve a non-local contraction of the entire tensor network, for which non-local approximate algorithms are necessary [83, 84].

However, the biggest challenge in formulating an EmQM theory using a tensor network algorithm is that so far, no (local or nonlocal) time-evolving tensor network algorithm has been shown to be robust enough to create high-complexity states (*e.g.* those created during the quantum advantage experiments [9–12]) with fixed bond dimension. With sufficiently large bond dimension, most tensor network algorithms can simulate essentially anything. However in EmQM, we would like to imagine that the bond dimension is fixed and not too large. Instead, it is the distance between physical qubits and time over which the dynamics occurs that is large, and it is over these extremely large scales that perhaps quantum mechanics could emerge.

⁷ However, extra spatial dimensions could be used to solve this bounded entanglement problem [27].

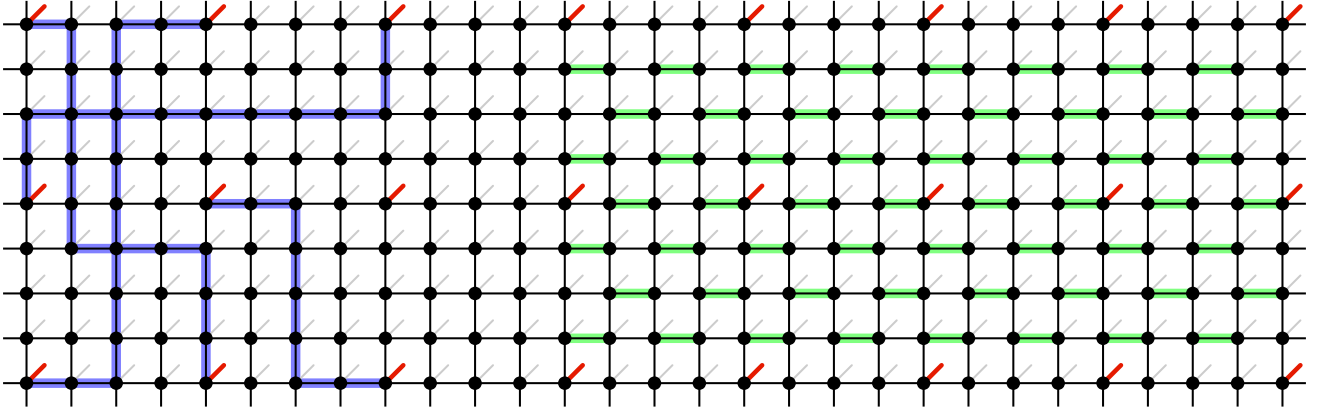


FIG. 8. A PEPS with physical qubits (dangling red lines) separated by many unimportant qubits (dangling gray lines), which we consider unimportant after coarse-graining. Black dots represent tensors which are contracted along the black lines. We see that the PEPS can easily represent many well-separated by Bell states by threading their entanglement along the blue lines. Furthermore, unitary circuits can be embedded into the PEPS (with unitary gates encoded in tensor pairs highlighted in green) to encode high-complexity states.

Appendix E: Bell's Theorem and Tensor/Neural Networks

Bell's theorem [85] and its conceptually simpler⁸ GHZ variant [86–88] show that local hidden variable theories are incompatible with quantum mechanics. In Appendix E 1 we review the GHZ variant. In Appendix E 2 we then discuss why tensor networks and neural networks are not local hidden variable theories [spoiler: Eqs. (E4) and (E6) are not satisfied] and can therefore bypass Bell's theorem (and its variants). Invoking a superdeterminism [89] loophole [90] is not necessary.

1. Review: GHZ Variant of Bell's Theorem

Writing the 3-qubit GHZ state in the ZZZ, YYX, and XXX basis yields:

$$\begin{aligned}
 |\psi\rangle &= \frac{1}{\sqrt{2}}|+z+z+z\rangle + \frac{1}{\sqrt{2}}|-z-z-z\rangle && \text{ZZZ basis} \\
 &= \frac{1}{2}|-y-y-x\rangle + \frac{1}{2}|-y+y+x\rangle + \frac{1}{2}|+y-y+x\rangle + \frac{1}{2}|+y+y-x\rangle && \text{YYX basis} \\
 &= \frac{1}{2}|+x+x+x\rangle + \frac{1}{2}|+x-x-x\rangle + \frac{1}{2}|-x+x-x\rangle + \frac{1}{2}|-x-x+x\rangle && \text{XXX basis}
 \end{aligned} \tag{E1}$$

$|\psi\rangle$ takes a similar permuted form in the YXY and XYY basis. We use the following notation for the qubit states

$$\begin{aligned}
 |\pm_x\rangle &= \frac{1}{\sqrt{2}}|+z\rangle \pm \frac{1}{\sqrt{2}}|-z\rangle \\
 |\pm_y\rangle &= \frac{1}{\sqrt{2}}|+z\rangle \pm \frac{i}{\sqrt{2}}|-z\rangle
 \end{aligned} \tag{E2}$$

which are eigenstates of the Pauli operators: $\hat{\sigma}^\mu|\pm_\mu\rangle = \pm|\pm_\mu\rangle$. In this Appendix, operators will always be denoted with a hat. Note that the GHZ state has a fixed measurement outcome for the $\hat{Y}_1\hat{Y}_2\hat{X}_3$ and $\hat{X}_1\hat{X}_2\hat{X}_3$ operators (along with permutations)

$$\begin{aligned}
 \langle\psi|\hat{Y}_1\hat{Y}_2\hat{X}_3|\psi\rangle &= -1 \\
 \langle\psi|\hat{X}_1\hat{X}_2\hat{X}_3|\psi\rangle &= +1
 \end{aligned} \tag{E3}$$

\hat{X}_i denotes the $\hat{\sigma}^x$ Pauli operator acting on the i^{th} qubit, and similar for \hat{Y}_i and \hat{Z}_i .

⁸ The GHZ variant is simpler in the sense that every measurement outcome is fixed according to quantum mechanics and simultaneously inconsistent with a local hidden variable theory. In contrast, Bell's original theorem only establishes a probabilistic Bell inequality. However, the GHZ variant involves three qubits instead of two.

In a hidden variable theory⁹, measurement outcomes only depend on a hidden classical variable h , which has a probability density $P(h)$. The measurement outcome due to measuring a qubit i in the X, Y, or Z basis can then be written as:

$$\begin{aligned} X_i(h) &= \pm 1 \\ Y_i(h) &= \pm 1 \\ Z_i(h) &= \pm 1 \end{aligned} \tag{E4}$$

Therefore, the quantum expectation values reduce to classical expectation values:

$$\begin{aligned} \langle \psi | \hat{X}_i | \psi \rangle &= \int_h P(h) X_i(h) \\ \langle \psi | \hat{Y}_i | \psi \rangle &= \int_h P(h) Y_i(h) \\ \langle \psi | \hat{Z}_i | \psi \rangle &= \int_h P(h) Z_i(h) \end{aligned} \tag{E5}$$

In a *local* hidden variable theory, measuring qubit i can not affect the measurement outcome of qubit j if qubit j is far away and measured immediately after qubit i . Therefore, for space-like separated measurements in a local hidden variable theory, the multi-point quantum expectation values also reduce to analogous classical expectation values; in particular:

$$\begin{aligned} \langle \psi | \hat{Y}_1 \hat{Y}_2 \hat{X}_3 | \psi \rangle &= \int_h P(h) Y_1(h) Y_2(h) X_3(h) \\ \langle \psi | \hat{X}_1 \hat{X}_2 \hat{X}_3 | \psi \rangle &= \int_h P(h) X_1(h) X_2(h) X_3(h) \end{aligned} \tag{E6}$$

To obtain a contradiction with quantum theory, note that Eqs. (E3), (E4), (E6), and permutations imply that

$$Y_1(h) Y_2(h) X_3(h) = Y_1(h) X_2(h) Y_3(h) = X_1(h) Y_2(h) Y_3(h) = -1 \tag{E7}$$

$$X_1(h) X_2(h) X_3(h) = +1 \tag{E8}$$

for all hidden variables h (with $P(h) \neq 0$). However, $X_1(h) X_2(h) X_3(h)$ can be rewritten using Eq. (E7)

$$\begin{aligned} X_1(h) X_2(h) X_3(h) &= [Y_1(h) Y_2(h) X_3(h)] [Y_1(h) X_2(h) Y_3(h)] [X_1(h) Y_2(h) Y_3(h)] \\ &= [-1][-1][-1] = -1 \end{aligned} \tag{E9}$$

since $Y_i(h)^2 = 1$. The above Eq. (E9) contradicts Eq. (E8). This shows that quantum mechanics can not be described by a local hidden variable theory.

2. Tensor and Neural Networks

Tensor networks and neural networks might seem like hidden variable theories. However, neither are local hidden variable theories and are therefore not ruled out by Bell experiments. The primary issue is that observables are not well-defined in terms of hidden variables, as in Eq. (E4), in tensor or neural networks.

Furthermore, in the limit of infinite bond dimension or number of training parameters, tensor and neural networks can simulate quantum mechanics exactly [30, 37, 92], which implies that Bell's theorem must not be violated in that limit. If an exact tensor or neural network (or other EmQM theory in an exact limit) were to simulate a Bell experiment, then there would be no sense of local realism. That this, after the observers measured their qubits, the EmQM theory would be encoding a wavefunction that consists of a superposition of measurement outcomes, as predicted by Schrödinger's equation. As emphasized in the many-worlds interpretation of quantum mechanics, the wavefunction would then approximately consist of multiple "branches" that evolve independently in superposition

⁹ Other definitions of hidden variable theories exist in the literature [91]. We are reviewing the definition as used in Bell's theorem.

since they are extremely unlikely to interfere with each other¹⁰. In an actual non-exact EmQM theory, only a limited number of wavefunction branches could be retained. Therefore, *after* the measurements took place, an EmQM theory would eventually be forced to randomly drop wavefunction branches (especially if many Bell measurements are performed). As long as only valid branches are retained and branches are dropped with the correct probability, the Bell experiments would not notice deviations from quantum mechanics. In a matrix product state (MPS) tensor network, dropping a branch could be achieved by a special random (or pseudo-random) truncation of a bond dimension.

a. GHZ Example

For example, the 3-qubit GHZ state from Eq. (E1) can easily be encoded in a matrix product state (MPS) tensor network in the ZZZ basis:

$$|\psi\rangle = \sum_{a_1, a_2, a_3, \alpha, \beta=0,1} A_{a_1, \alpha} B_{\alpha, a_2, \beta} C_{\beta, a_3} |a_1 a_2 a_3\rangle \quad (\text{E10})$$

$$\begin{aligned} A_{a_1, \alpha} &= \delta_{a_1, \alpha} \\ B_{\alpha, a_2, \beta} &= 2^{-1/2} \delta_{\alpha, a_2, \beta} \\ C_{\beta, a_3} &= \delta_{\beta, a_3} \end{aligned} \quad (\text{E11})$$

where (a_1, a_2, a_3) index states in the Z basis ($|0\rangle = |+_z\rangle$ and $|1\rangle = |-_z\rangle$) and (α, β) are virtual indices. δ is the Kronecker delta, with $\delta_{a,b,c} = 1$ if $a = b = c$ else $\delta_{a,b,c} = 0$.

One could attempt to map the above tensor network to a hidden variable theory by defining the hidden variable as the physical and virtual indices: $h = (a_1, a_2, a_3, \alpha, \beta)$. Then the Z-basis measurements obey the analogs of Eqs. (E4–E6) with $P(h) = \frac{1}{2} \delta_{a_1, a_2, a_3, \alpha, \beta}$ and $Z_i(h) = (-1)^{a_i}$. However, there is no choice of $X_i(h)$ and $Y_i(h)$ that is also consistent with Eqs. (E4–E6).¹¹

Neural networks also fail to be a local hidden variable theory in a similar way.

¹⁰ This assumes that the observers (including the surrounding environment) consist of many chaotic degrees of freedom, which is certainly true for human observers.

¹¹ One might alternatively imagine adding α' and β' to the hidden variable in order to account for virtual indices for a bra state. However, this does not help turn the tensor network into a local hidden variable theory.